Journal of Biomedical Optics

SPIEDigitalLibrary.org/jbo

Polarization-sensitive optical coherence tomography using continuous polarization modulation with arbitrary phase modulation amplitude

Zenghai Lu
Deepa K. Kasaragod
Stephen J. Matcher

SPIE

Polarization-sensitive optical coherence tomography using continuous polarization modulation with arbitrary phase modulation amplitude

Zenghai Lu, Deepa K. Kasaragod, and Stephen J. Matcher
University of Sheffield, Department of Materials Science & Engineering, Sheffield, S3 7HQ, UK

Abstract. We demonstrate theoretically and experimentally that the phase retardance and relative optic-axis orientation of a sample can be calculated without prior knowledge of the actual value of the phase modulation amplitude when using a polarization-sensitive optical coherence tomography system based on continuous polarization modulation (CPM-PS-OCT). We also demonstrate that the sample Jones matrix can be calculated at any values of the phase modulation amplitude in a reasonable range depending on the system effective signal-to-noise ratio. This has fundamental importance for the development of clinical systems by simplifying the polarization modulator drive instrumentation and eliminating its calibration procedure. This was validated on measurements of a three-quarter waveplate and an equine tendon sample by a fiber-based swept-source CPM-PS-OCT system. [DOI: 10.1117/1.JBO.17.3.030504]

Keywords: phase modulation amplitude; polarization-sensitive optical coherence tomography; polarization modulator.

Paper 11713L received Dec. 2, 2011; revised manuscript received Jan. 10, 2012; accepted for publication Jan. 11, 2012; published online Mar. 8, 2012.

1 Introduction

Polarization-sensitive optical coherence tomography (PS-OCT) is a functional extension of OCT and has been used extensively to image birefringent biological tissues.[1] Recently PS-OCT with continuous polarization modulation (CPM-PS-OCT) has been reported,[2,3] in which CPM is required to obtain frequency-shifted OCT signals with respect to the modulation frequency. An electro-optic modulator (EOM) is typically necessary to modulate the polarization state of the sample illuminating light continuously. The phase modulation of the EOM is $\varphi = A\sin(\omega_m t)$, where ω_m is the angular frequency of CPM. It is customary to choose the EOM phase modulation amplitude of $A = A_0 = 2.405$ radians in CPM-PS-OCT, so that the zero'th-order of the Bessel function of the first kind is evaluated to be zero, namely, $J_0(A_0) = 0$.[2]

To achieve this condition, the EOM must be carefully calibrated to ensure that $A = A_0$. For this calibration, Jiao et al.[2] proposed an approach, in which the ratio of the intensities of the $2\omega_m$ and the $4\omega_m$ harmonics of the EOM modulation frequency in both detection channels was measured and ensured to be $J_2(A_0)/J_4(A_0) = 6.667$. However, it is extremely difficult to use this calibration method when a resonant EOM is used since the detection of the harmonics is typically limited by the data acquisition speed. This is because the resonant frequency ω_m is typically set between 1/3 and 1/2 of the data acquisition speed to optimize the system measurement depth range. Todorović et al.[4] pointed out that a phase modulation amplitude other than A_0 could in principle be used provided that the EOM does not saturate at any point. However, theoretical and experimental studies on this have not been presented to date. In this letter, we present theoretical and experimental analysis on the use of different phase modulation amplitude for CPM-PS-OCT measurements, and show that the optic axis orientation and phase retardance of a sample can be calculated without prior knowledge of the actual value of the phase modulation amplitude provided that the amplitude is in a reasonable range. This eliminates the need for the EOM calibration process and allows the use of any phase modulation amplitude that does not saturate the EOM. These conclusions are validated by measurements on a three-quarter waveplate (TQWP) and equine tendon using a CPM-PS-OCT system.

2 System and Theory

The CPM-PS-OCT system used in this work has been described in our previous paper.[5] Briefly, the light source was a 10 kHz wavelength sweeping laser (HSL-2000, Santec) which sweeps over 128 nm across a center wavelength of 1.3 μm. The light is polarized by a linear polarizer and then modulated continuously by a broadband waveguide EOM (PC-B3-00-SFAP-SFA-130-U, EOSpace). The modulated light is split into the reference and sample arm and recombined and detected. The theoretical description and data processing procedures of the system have been described in details elsewhere.[2,3] When the EOM amplitude is adjusted to a value of A_0 the depth-resolved Jones matrices of the combined system fibers and sample are algebraically calculated from the experimental data,

$$J_{\text{measured}} = \begin{bmatrix} -\tilde{I}^*_{h0} - \frac{\tilde{I}^*_{h1}}{J_1(A_0)} & \tilde{I}^*_{h0} - \frac{\tilde{I}^*_{h1}}{J_1(A_0)} \\ -\tilde{I}^*_{v0} - \frac{\tilde{I}^*_{v1}}{J_1(A_0)} & \tilde{I}^*_{v0} - \frac{\tilde{I}^*_{v1}}{J_1(A_0)} \end{bmatrix}, \quad (1)$$

where $\tilde{I}^*_{h0}$, $\tilde{I}^*_{h1}$, $\tilde{I}^*_{v0}$, $\tilde{I}^*_{v1}$ shows the complex conjugate of the horizontally polarized nonmodulated, first-order, vertically polarized nonmodulated, first-order OCT signals, respectively, and $J_1(A_0)$ is the first-order Bessel function of the first kind evaluated at A_0.[3] However, when the amplitude is set to a general value A, we use the Jones matrix-based analysis of PS detection in CPM-PS-OCT[2,3] to deduce a general expression for J_{measured},

Address all correspondence to: Zenghai Lu, University of Sheffield, Department of Materials Science & Engineering, Sheffield, S3 7HQ, UK. Tel: 44 114 2225994; E-mail: z.lu@sheffield.ac.uk

0091-3286/2012/$25.00

$$J_{\text{measured}} = \begin{pmatrix} -\tilde{I}^*_{h0} - \frac{\tilde{I}^*_{h1}}{J_1(A)}[1+J_0(A)] & \tilde{I}^*_{h0} - \frac{\tilde{I}^*_{h1}}{J_1(A)}[1-J_0(A)] \\ -\tilde{I}^*_{v0} - \frac{\tilde{I}^*_{v1}}{J_1(A)}[1+J_0(A)] & \tilde{I}^*_{v0} - \frac{\tilde{I}^*_{v1}}{J_1(A)}[1-J_0(A)] \end{pmatrix}, \quad (2)$$

where $J_0(A)$, $J_1(A)$ are the zero'th and the first-order Bessel function of the first kind evaluated at the set phase modulation amplitude A, respectively. Equation (2) shows that in principle A can be set to an arbitrary value provided that the EOM is not saturated at any point, i.e., J_{measured} measured can be calculated with any values of A. The limit for small values of A depends on the system sensitivity since the system would show large measurement uncertainty when the generated first-order OCT signal approaches the system noise floor.

Both Eqs. (1) and (2) show, however, that the value of A must be known in order to recover the desired Jones matrices from the measurement data $\tilde{I}^*_{h0}$, etc. This requires that the EOM must be carefully calibrated. In practice, it is also necessary to compensate the fiber-induced birefringence in the sample arm fiber. To do this, the Jones matrix at the sample surface J_{sur} is used as a reference matrix to calculate the birefringence in the sample. The double-pass phase retardance η and fast-axis orientation θ of the sample can then be obtained from the matrix diagonalization of the following equation (Ref. 6),

$$J_{c,m} = J_{\text{measured}} J_{\text{sur}}^{-1} = J_U \begin{pmatrix} p_1 e^{i\eta/2} & 0 \\ 0 & p_1 e^{-i\eta/2} \end{pmatrix} J_U^{-1}, \quad (3)$$

where p_1, p_2 are two transmittances of the eigenvectors of the sample, and J_U is a general unitary matrix, whose columns are the fast and slow eigenpolarizations of $J_{c,m}$. θ is extracted from these eigenpolarizations. The degree of the phase retardance can be extracted through the phase difference of the resulting diagonal elements. We will now show that this surface calibration procedure in fact completely cancels the effects of varying of the value of A, i.e., $J_{c,m}$ can be calculated without knowing the actual value of A. To do this, we first note Eq. (2) can be matrix-factorized into the following form:

$$J_{\text{measured}} = J_{\text{sig}} J_i J_{B1}(A) J_{B0}(A),$$

where

$$J_{\text{sig}} = \begin{pmatrix} \tilde{I}^*_{h0} & \tilde{I}^*_{h1} \\ \tilde{I}^*_{v0} & \tilde{I}^*_{v1} \end{pmatrix}, \quad J_i = \begin{pmatrix} -1 & 1 \\ -1 & -1 \end{pmatrix},$$

$$J_{B1}(A) = \frac{1}{2}\begin{pmatrix} 1+\frac{1}{J_1(A)} & \frac{1}{J_1(A)}-1 \\ \frac{1}{J_1(A)}-1 & 1+\frac{1}{J_1(A)} \end{pmatrix}, \quad (4)$$

$$J_{B0}(A) = \begin{pmatrix} 1+\frac{J_0(A)}{2} & -\frac{J_0(A)}{2} \\ \frac{J_0(A)}{2} & 1-\frac{J_0(A)}{2} \end{pmatrix}.$$

Here, we define three new Jones matrices: J_{sig}, $J_{B0}(A)$, and $J_{B1}(A)$. Note that J_{sig} is determined solely by the experimentally measured signals $\tilde{I}^*_{h0}$, etc. $J_{B0}(A)$, $J_{B1}(A)$ are determined solely by the values of the Bessel functions at the value A and J_i is a constant Jones matrix. $J_{B0}(A)$ becomes the identity matrix and Eq. (4) reduces to Eq. (1) when $A = A_0$. $J_{B0}(A)$, $J_{B1}(A)$ are clearly invertible matrices. Substituting Eq. (4) into Eq. (3)

$$\begin{aligned} J_{c,m} &= J_{\text{measured}} J_{\text{sur}}^{-1} \\ &= (J_{\text{sig}} J_i J_{B1}(A) J_{B0}(A))(J_{\text{sigsur}} J_i J_{B1}(A) J_{B0}(A))^{-1} \\ &= J_{\text{sig}} J_{\text{sigsur}}^{-1}, \end{aligned} \quad (5)$$

where J_{sigsur} corresponds to J_{sig} as measured at the sample surface. Equation (5) shows that the calibrated Jones matrix $J_{c,m}$, which by Eq. (3) contains all the information needed to determine the sample phase retardance and relative optic-axis orientation, can be derived purely from the experimentally measured signals $\tilde{I}^*_{h0}$, etc. at the desired depth as well as at the surface. The value of A is not specifically required and this makes it possible to avoid the EOM calibration process. Values of $A < 2.405$ can also be used, which can simplify the provision of the EOM drive voltage.

3 Experimental Results

A single-plate TQWP (WPF410, CryLight) was used as a test target to validate the theoretical analysis in previous section using our system. The phase modulation amplitude, A, of the EOM used was first calibrated by using a generalized analysis based upon previous reports[7] and the measured half-wave voltage of the EOM was 9.5 V. Therefore, the different values of A could be set manually by slowly adjusting the drive voltage. It should be noted that this calibration method is limited for the specific EOM used (i.e., waveguide based) and thus has limitation in terms of generality and practicality. In this measurement, A was set from ~3.20 to 0 radians with a 0.23 radians increment (equivalent to 2 V peak-to-peak drive voltage). The sample Jones matrix was calculated without knowledge of the actual value of A by using Eq. (5) and the results are shown in Fig. 1, in which relative fast-axis orientation was calculated using the method proposed in Ref. 6. The TQWP was kept untouched during the measurement. Figure 1 shows the measured phase retardance (left) and optic-axis orientation (right) along with the standard deviation of each measurement as functions of A. Several tens of A-scans were collected at each A during the experiment and the results were used to calculate the standard deviation of the measurement. It is clear that the measured retardance and orientation are essentially the same when A varies from ~0.65 to 3.20 radians, suggesting that the measurement of phase retardance and orientation is indeed independent of A. The systematic measurement error and the standard deviation increase when A falls below

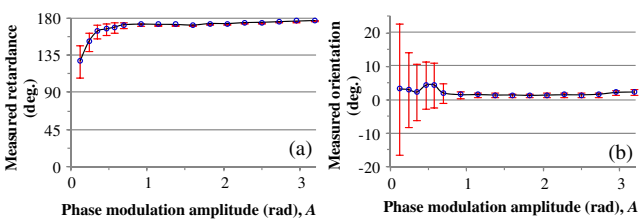

Fig. 1 Measured phase retardance (a) and relative orientation (b) of the TQWP for different values of the phase modulation amplitude, A. Several tens of A-scans were collected at each value of A and used for calculating the standard deviation of the measurement

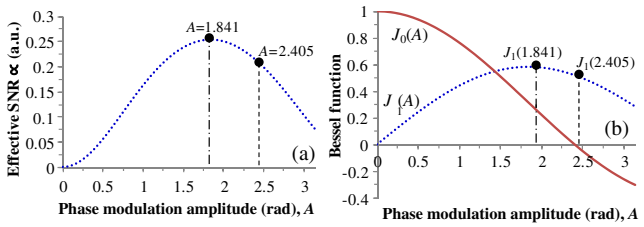

Fig. 2 (a) Plot of the system effective SNR as a function of phase modulation amplitude, A. (b) Plot of zero- and first-order Bessel functions of the first kind as a function of A. Bessel functions were calculated using MatLab function 'Besselj.'

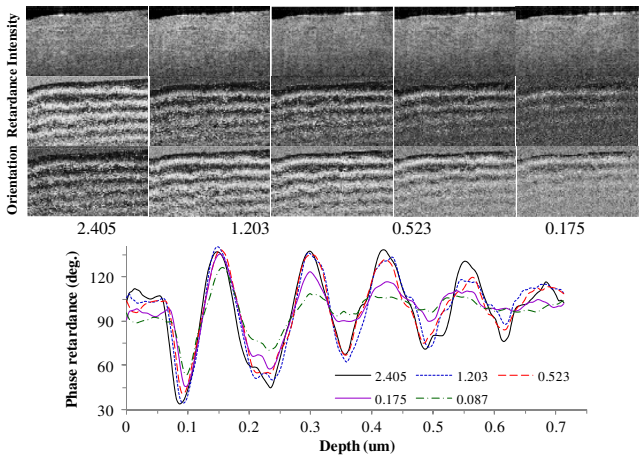

Fig. 3 Measured intensity, phase retardance, and orientation images (top) of equine tendon against A. Profiles of phase retardance images are included (bottom). Measured intensity, phase retardance and orientation images of equine tendon against A. Averaged profiles of phase retardance images are included (bottom).

~0.65 radian. This is because the phase retardance error depends on the effective signal-to-noise ratio (SNR) of the measurement, which is inversely proportional to $[1 + 1/J_1^2(A)]$ (Ref. 8), as shown in Fig. 2(a). Our system sensitivity was measured to be ~107 dB near zero optical path difference. Improving the system sensitivity can possibly extend the effective range of A that yields accurate measurements. It should be stressed that the measured phase retardance and orientation in Fig. 1 do change with the value of A when A reduces from ~0.65 radian, although Eq. (2) shows in principle the Jones matrix of the sample can be calculated with any values of A and the calculated value is independent of A. This does not indicate that the measurement results depend on the value of A because the change of the measurement results is due to the decreasing of the system effective SNR leading to the significant increasing of the measurementuncertainty.

A birefringent biological tissue, equine tendon, was also used as a test target. The sample surface was oriented orthogonal to the incident beam and the results are shown in Fig. 3. It is clearly seen that the phase retardance and orientation images are essentially the same when the phase modulation amplitude A varies from 2.405 to ~0.5 radians. For a quantitative analysis, the averaged profile of the phase retardance image was obtained by lateral averaging 100 A-scans in the image at each value of A and shown in Fig. 3 (bottom). It is clear that the reasonable image quality can be obtained for $A > \sim 0.5$ radian, requiring a peak-to-peak AC drive voltage of ~4 V. This voltage could easily be provided by a typical function generator itself or an analog output card with no auxiliary amplifier being required.

4 Conclusions

In conclusion, both theory and experiment have demonstrated that the phase modulation amplitude of the EOM has limited effect on the measurement in CPM-PS-OCT over a large range of values and furthermore that using surface calibration to remove fiber birefringence effects also removes the need to explicitly know the value of A. In actual applications, the practical upper limit for A is set by the required drive voltage which depends on electronic constraints and also on the type of modulator (especially crystal versus waveguide). The limit for small values of the amplitude depends on the system sensitivity and sample optical properties since the system will show large measurement uncertainty and systematic errors when the generated first-order OCT signal is close to/below the system noise floor. The effective SNR of the system is proportional to the square of the first-order Bessel function of the first kind evaluated at A. Therefore, the optimal working point of the EOM in CPM-PS-OCT is at a phase modulation amplitude whose first-order Bessel function of the first kind is maximized i.e., $A = 1.841$ as shown in Fig. 2(b). This could allow simpler EOM drive electronics and improved SNR compared with the current widely used value of $A = 2.405$.

Acknowledgments

The authors acknowledge the contributions of M Yamanari and Y Yasuno from Tsukuba University in developing the system. This research was supported by EPSRC Grant EP/F020422.

References

1. J. F. deBoesr et al., "Two-dimensional birefringence imaging in biological tissue by polarization-sensitive optical coherence tomography," *Opt. Lett.* **22**(12), 934–936 (1997).
2. S. L. Jiao et al., "Fiber-based polarization-sensitive Mueller matrix optical coherence tomography with continuous source polarization modulation," *Appl. Opt.* **44**(26), 5463–5467 (2005).
3. M. Yamanari, S. Makita, and Y. Yasuno, "Polarization-sensitive swept-source optical coherence tomography with continuous source polarization modulation," *Opt. Express* **16**(8), 5892–5906 (2008).
4. M. Todorovic et al., "In vivo burn imaging using Mueller optical coherence tomography," *Opt. Express* **16**(14), 10279–12084 (2008).
5. Z. H. Lu, D. K. Kasaragod, and S. J. Matcher, "Optic axis determination by fibre-based polarization-sensitive swept-source optical coherence tomography," *Phys. Med. Biol.* **56**(4), 1105–1122 (2011).
6. B. H. Park et al., "Jones matrix analysis for a polarization-sensitive optical coherence tomography system using fiber-optic components," *Opt. Lett.* **29**(21), 2512–2514 (2004).
7. F. Heismann, "Analysis of a reset-free polarizatoin controller for fast automatic polarization stabilization in fiberoptic transmission-systems," *J. Lightwave Technol.* **12**(4), 690–699 (1994).
8. S. Makita, M. Yamanari, and Y. Yasuno, "Generalized Jones matrix optical coherence tomography: performance and local birefringence imaging," *Opt. Express* **18**(2), 854–876 (2010).